http://dx.doi.org/10.5012/bkcs.2013.34.11.3362

Separation of Selenite from Inorganic Selenium Ions using TiO_2 Magnetic Nanoparticles

Jongmin Kim and H. B. Lim*

*Department of Chemistry, NSBI, Dankook University, Gyeonggi-do 448-701, Korea. *E-mail: plasma@dankook.ac.kr*
Received June 14, 2013, Accepted August 27, 2013

A simple and quick separation technique for selenite in natural water was developed using TiO_2@SiO_2/Fe_3O_4 nanoparticles. For the synthesis of nanoparticles, a polymer-assisted sol-gel method using hydroxypropyl cellulose (HPC) was developed to control particle dispersion in the synthetic procedure. In addition, titanium butoxide (TBT) precursor, instead of the typical titanium tetra isopropoxide, was used for the formation of the TiO_2 shell. The synthesized nanoparticles were used to separate selenite (Se^{4+}) in the presence of Se^{6+} or selenium anions for the photocatalytic reduction to Se^0 atom on the TiO_2 shell, followed by magnetic separation using Fe_3O_4 nanoparticles. The reduction efficiency of the photocatalytic reaction was 81.4% at a UV power of 6W for 3 h with a dark adsorption of 17.5% to the nanoparticles, as determined by inductively coupled plasma-mass spectrometry (ICP-MS). The developed separation method can be used for the speciation and preconcentration of selenium cations in environmental and biological analysis.

Key Words : Selenium ions, Separation, TiO_2 nanoparticle, Selenite

Introduction

Selenium is a well-known, naturally occurring trace element that can exist in either inorganic forms or as organic species. It is primarily present in four different oxidation states: selenide (Se^{2-}), elemental selenium (Se^0), selenite (Se^{4+}) and selenate (Se^{6+}). The inorganic species changes their form depending upon the pH of the solution as Se^{2-}, SeO_3^{2-} and SeO_4^{2-}, and their protonated anions. Among them, selenite and selenate are more toxic than the other inorganic forms. Therefore, the speciation of selenium has become an important issue in environmental and biological analysis. However, the complexity of selenium speciation has rendered it one of the interesting challenges in analytical separation.[1]

The most common separation technique is HPLC including ion-exchange chromatography, reverse-phase chromatography, and size-exclusion chromatography, hyphenated with atomic spectrometry, such as inductively coupled plasma-atomic emission spectrometry (ICP-AES), ICP-mass spectrometry (ICP-MS), graphite furnace atomic absorption spectrometry, and atomic fluorescence spectrometry.[2] Preconcentration is also an issue in the speciation, for which liquid-liquid extraction, solid phase extraction,[3] ion-exchange,[4] and coprecipitation[5] are the traditional techniques. However, these techniques suffer from complexity and long analysis time.

In this work, we propose a simple and quick separation technique to speciate selenite by photocatalytic reduction. Since selenium has multiple oxidation states, it participates in various redox reactions. For example, selenite and selenate can be reduced to Se^0 by photocatalytic reaction of TiO_2 materials.[6-9] The photocatalytic reaction can be achieved by the irradiation of either solar radiation[10] or a UV light source ($\leq$ 385 nm)[11] on TiO_2 shell that can generate electron–hole pairs (e–/h+) owing to its large band gap of around 3.2 eV.

Despite TiO_2 nanoparticles being an excellent material to reduce Se cations in aqueous solution, the reduced selenium atoms on the nanoparticles should be removed or re-collected completely because they can induce secondary contamination. They are commonly removed by the sedimentation of TiO_2 particles after pH adjustment and coagulation–flocculation. However, those methods required further microfiltration for final purification.[12,13] Therefore, TiO_2-coated Fe_3O_4 magnetic nanoparticles are the choice to overcome the current drawbacks. The superparamagnetic property of the core Fe_3O_4 provides not just only magnetic separation in the presence of external magnetic force but also good stability in aqueous solution at relatively low production cost.[10,14] In addition, the presence of the insulation SiO_2 layer between the magnetic core and the TiO_2 shell prevents photodissolution of iron and enhances the stability in aqueous solution under UV illumination.[15] Furthermore, the intermediate SiO_2 barrier prevented the magnetic core from acting as an electron–hole recombination center, which can negatively affect the photocatalytic activity.[16,17] So far, Beydoun *et al.* have been pioneers in discussing the synthesis and characterization of these magnetic nanoparticles for photocatalytic reaction.[18-21] However, no report has been published on the application of TiO_2@SiO_2/Fe_3O_4 nanoparticles to the separation of selenium cations.

In this work, therefore, we develop a unique polymer-assisted sol-gel method for TiO_2@SiO_2/Fe_3O_4 nanoparticles. For this, hydroxypropyl cellulose (HPC) polymer is used to control the particle dispersion. In addition, titanium butoxide (TBT), instead of the typical titanium isopropoxide, is used for the formation of TiO_2 shell on the Fe_3O_4 nanoparticles.

Again, the synthesized TiO_2@SiO_2/Fe_3O_4 nanoparticles had two noticeable functionalities: photocatalytic reduction of selenium cations to Se^0 atoms by TiO_2 shell and an attractive superparamagnetic force for the particle collection by Fe_3O_4 core. The synthesized nanoparticles are characterized by scanning electron microscopy (SEM), X-ray diffraction (XRD) and energy dispersive X-ray spectroscopy (EDAX) and then used to study the separation of selenite from inorganic selenium ions in natural water in the presence of formic acid as a hole scavenger. The separation efficiency is estimated by determining the remained selenium ions in the sample solution and the coated selenium atoms on the nanoparticles using ICP-MS.

Experimental

Synthesis of SiO_2@Fe_3O_4 Magnetic Nanoparticles. Silica-coated Fe_3O_4 magnetic nanoparticles (SiO_2@Fe_3O_4) were synthesized by the alkaline co-precipitation of $FeCl_3 \cdot 6H_2O$ and $FeCl_2 \cdot 4H_2O$, as described in our previous article.[22] Under the argon gas flowing condition, $FeCl_2 \cdot 4H_2O$ (0.5 g) and $FeCl_3 \cdot 6H_2O$ (1.35 g) were dissolved in 25 mL of de-ionized water. Then, 12.5 mL ammonium hydroxide (28-30%, Sigma-Aldrich Chem. Co., USA) was added while the solution was heated at 80 °C for 20 min. The synthesized Fe_3O_4 magnetic nanoparticles were washed three times with ethanol and de-ionized water under magnetic separation. The silica shell was formed by a Stober method using tetra-ethyl orthosilicate (TEOS; 99.999%, Sigma-Aldrich Chem. Co., USA). For this, 350 mg of Fe_3O_4 magnetic nanoparticles was added to 30 mL of anhydrous ethanol in a round bottom flask and dispersed by sonication and vortexing. After adding 520 μL of ammonium hydroxide and de-ionized water, the nanoparticles were re-dispersed. Then, 3.3 mL of TEOS was added under flowing argon gas and reacted for 90 min. The synthesized SiO_2@Fe_3O_4 magnetic nanoparticles were washed three times with ethanol and de-ionized water, and then stored at ethanol.

Preparation of TiO_2@SiO_2/Fe_3O_4 Nanoparticles. In the sol-gel method used for TiO_2 coating, a 500 mL round bottom flask equipped with a reflux column, a thermometer, and needle ports for nitrogen gas was prepared. The chemical reagents were supplied by a peristaltic pump through a needle. The reaction proceeded by mixing 0.1 g of SiO_2@Fe_3O_4 nanoparticles with 7.5 mL of ammonium hydroxide, 6 mL of de-ionized water, and 250 mg of HPC polymer using a magnetic stirrer for 10 min under the inert condition of N_2 gas. Then, 2 mL of TBT (reagent grade, 97%, Sigma-Aldrich Chem. Co., USA) in 23 mL of ethanol with ammonium hydroxide (28-30%, Sigma-Aldrich Chem. Co., USA) was added at the flow rate of 2.5 mL/min. The solution was refluxed for 90 min at 85 °C. After cooling to room temperature, the TiO_2@SiO_2/Fe_3O_4 magnetic nanoparticles were washed three times with ethanol and the final powder was sintered in an electrical muffle furnace for 2 h at 400 °C.

Photocatalytic Reaction of Se Ions. For the photocatalytic reaction, the standard solutions of Se^{4+}, Se^{6+}, and Se^{2-} were prepared by dissolving Na_2SeO_3 (sodium selenite, 99%, Sigma-Aldrich Chem. Co., USA), $Na_2SeO_4 \cdot 10H_2O$ (sodium selenate decahydrate, 99.999%, Sigma-Aldrich Chem. Co., USA), and dimethyl diselenide, (96%, Sigma-Aldrich Chem. Co., USA) in deionized water. Formic acid (98%, Sigma-Aldrich Chem. Co., USA) was also used as a hole scavenger. The pH (Model: 420 A+, Orion, USA) was adjusted using NaOH (Sigma-Aldrich Chem. Co., USA) and de-ionized water (18.2 MΩ, Millipore-Q, USA). Photocatalytic reduction of the selenium cations was carried out at 25 °C in a bath mode of a rectangular quartz cell (10 × 10 × 30 mm). The reaction cell was directly irradiated by a low pressure D_2 lamp (6 Watt, Hamamatsu, Japan).

Table 1. Optimized operating condition of inductively coupled plasma-mass spectrometer (ICP-MS)

Instrument	DRC-e, PerkinElmer
RF power	1250 W
Acquisition mode	Peak hopping
Auxiliary gas flow	1.2 L min^{-1}
plasma gas flow	15 L min^{-1}
Nebulizer gas flow	0.96 L min^{-1}
Dwell time	20 ms
Lens voltage	7.5 V
DRC cell gas (CH_4)	0.6 L/min
Rpa (high mass cut-off)	0
Rpq (low mass cut-off)	0.9

Instruments. For the determination of ^{78}Se ions, an inductively coupled plasma-mass spectrometer (ICP-MS, Elan DRC-e, Perkinelmer Sciex) was used with a forward plasma power of 1.25 kW. Dynamic reaction cell (DRC) mode was used with CH_4 gas to suppress molecular interferences. The optimized experimental conditions are listed in Table 1. Standard solutions of Se for the calibration curves were prepared using ICP/DCP (direct current plasma) standard solution (9990 μg/mL, Aldrich) and 2% nitric acid for dilution.

Results and Discussion

Characterization of Superparamagnetic TiO_2@SiO_2/Fe_3O_4 Nanoparticles. Figure 1 presents TEM images of the synthesized TiO_2@SiO_2/Fe_3O_4 nanoparticles. As noted above, the synthesized nanoparticles offered two unique functionalities: photocatalytic reduction of selenium cations to Se^0 and an attractive superparamagnetic force. The superparamagnetic property of the Fe_3O_4 core was useful for simplifying the collection and washing due to the attractive force under a permanent magnet. As discussed, the TiO_2 shell was coated on the Fe_3O_4 nanoparticles (10-13 nm) for photocatalytic reduction. A SiO_2 layer was inserted prior to the TiO_2 coating to prevent degradation of the functional character of photocatalytic reduction with increasing irradiation time. The particle size was increased to within the range of 15 nm to 19 nm when the SiO_2 layer was coated, as shown in Figure 1(b). Figure 1(c) shows TEM images of

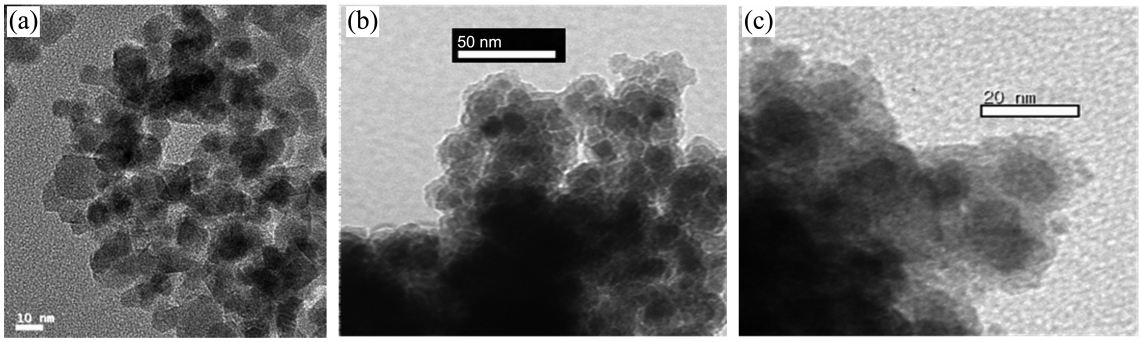

Figure 1. TEM images of the synthesized nanoparticles; (a) Fe_3O_4, (b) SiO_2/Fe_3O_4 and (c) $TiO_2@SiO_2/Fe_3O_4$.

$TiO_2@SiO_2/Fe_3O_4$ nanoparticles, with the coated TiO_2 layer being clearly evident as a core-shell type.

The chemical composite of the synthesized nanoparticles, as determined by EDAX, was listed in the Table 2. The analytical result revealed the presence of Fe, Si, Ti, and a significant amount of oxygen. The atomic percentage in the table indicates the number of atoms in the nanoparticles. The determined atom number of oxygen, 76.46%, is excessively larger than the other metal atoms, indicating that the metals existed as oxides. The similar number of Ti atoms and Fe atoms of the core indicated that the synthesized nanoparticles contained a sufficient Ti layer for photocatalytic activity, as well as superparamagnetic property of Fe_3O_4 core. Compared to the TiO_2 layer and the Fe_3O_4 core, the inserted SiO_2 layer was relatively thin.

For further structural information, XRD diffractograms before and after the coatings were obtained. As shown in Figure 2, the spectrum of the core Fe_3O_4 powders (Fig. 2(b)) dried at 80 °C was well matched with the standard XRD pattern (Fig. 2(a)) for bulk magnetite (JCPDS 19-06290). This typical magnetite pattern was seen even for the $TiO_2@SiO_2/Fe_3O_4$ nanoparticles, although the intensities were weakened as the coating was progressed. Since the SiO_2 layer was amorphous, no SiO_2 pattern was seen in this figure, but the weakening of the magnetite intensity after SiO_2 coating indicated the presence of the SiO_2 shell, which was further confirmed by the TEM image, as shown in Figure 1(b). Since the nanoparticles were calcinated at 400 °C after TiO_2 coating, the anatase XRD pattern of TiO_2 appeared along with the magnetite peaks as shown in Figure 2(d). The synthesized TiO_2 anatase pattern was confirmed with the standard pattern of JCPDS 21-1272 (peak A in Fig. 2(e)) for bulk anatase standard powder. To conclude, the synthesized nanoparticles had a core/shell/shell type with superparamagnetic and photocatalytic properties.

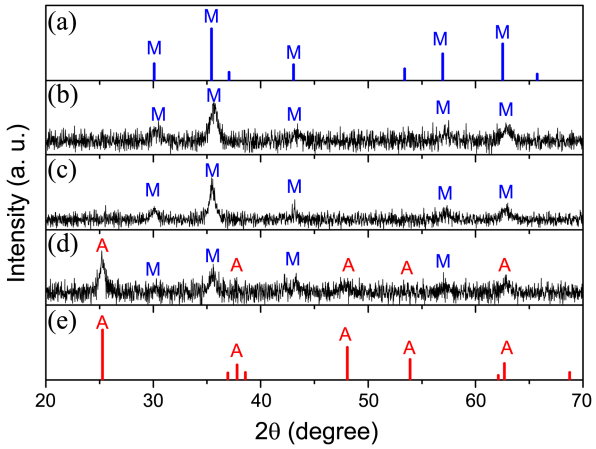

Figure 2. XRD patterns of (a) bulk magnetite (JCPDS 19-06290), (b) Fe_3O_4, (c) Fe_3O_4/SiO_2 (Core/shell), (d) $Fe_3O_4/SiO_2/TiO_2$ (Core/shell/shell), and (e) bulk anatase TiO_2 powder (JCPDS 21-1272).

Effect of HPC Polymer. In the coating procedure of the TiO_2 shell, HPC polymer was added to control the particle dispersion and size. As expected, the addition of HPC formed a boundary layer on the TiO_2 surface that functioned as a surfactant. Without the polymer addition, the nanoparticles became significantly large (> 150 nm) and their shape and size became difficult to control, as shown in Figure 3(a)). The large particles were probably formed by aggregation, resulting in multi-core nanoparticles. On the other hand, small particles (< 30 nm) were produced when the HPC polymer was added (Fig. 3(b)).

Table 2. Chemical composition of the $TiO_2@SiO_2/Fe_3O_4$ nanoparticles obtained using EDAX

Element	Weight%	Atomic%
O K	53.42	76.46
Si K	8.02	6.54
Ti K	17.38	8.31
Fe K	21.18	8.69
Totals	100	

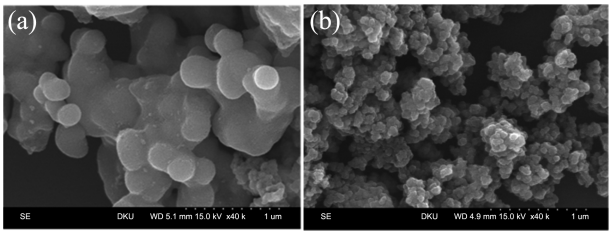

Figure 3. SEM images of $Fe_3O_4/SiO_2/TiO_2$ (Core/shell/shell) nanoparticles; (a) without HPC addition and (b) with HPC addition.

Photocatalytic Reduction of Selenium Cations. The synthesized TiO_2@SiO_2/Fe_3O_4 nanoparticles were used to separate and remove the toxic selenium cations selectively. After photocatalytic reaction of the inorganic selenium cations, the reduced selenium atoms were adsorbed on the TiO_2 surface and the nanoparticles were collected by magnetic separation. For demonstration, synthetic standard selenium solutions with oxidation states of +4 and +6 and selenium anions of −2 were prepared at pH 7.

Theoretical Insight on the Photocatalytic Reduction of Selenium Cations. The illumination of UV radiation on TiO_2 suspension is known to generate electrons and holes. While the holes are scavenged by the oxidation reaction of formic acid, the photogenerated electrons can participate in the reduction of metal ions. Since the reduction potential of the TiO_2 conduction band electron is about −0.2 eV in acidic condition,[23] it has enough energy to reduce selenite to selenium atom. The standard reduction potentials of selenium cations are shown in the following equation[24] although these redox potentials can be altered once they have been adsorbed on TiO_2 nanoparticles.

$$HSeO_3^- + 5H^+ + 4e = Se^0 + 3H_2O \quad E^0 = +0.780\ V \quad (1)$$

$$SeO_3^{2-} + 6H^+ + 4e = Se^0 + 3H_2O \quad E^0 = +0.903\ V \quad (2)$$

$$HSeO_3^- + 6e + 7H^+ \rightarrow H_2Se + 3H_2O \quad E^0 = +0.386\ V \quad (3)$$

According to the reactions (1) and (2), both the selenate and selenite can be thermodynamically reduced to selenium atoms that will be adsorbed on the surface of nanoparticles. Interestingly, the six-electron reduction of Se^{4+} to Se^{2-} is also possible because the reaction is thermodynamically feasible according to the reaction (3). Therefore, the production of Se^{2-} cannot be ruled out if the reducing power is sufficiently large enough. Therefore, the power of UV light source should be optimized for selective reduction of selenite to Se atoms. Too high power will produce anions that cannot be removed by the magnetic separation. In this study, a deuterium light source of 6 watts was used, which was small enough to minimize the production of selenium anions or even the reduction of selenate.

Dark Adsorption of Selenite. Before determination of the reduction efficiency, the electrostatic adsorption of selenite on the magnetic nanoparticles was studied to obtain dark adsorption as a background. For this, 20 μg/mL of selenite at pH 4 was mixed with 0.5 g/L of TiO_2@SiO_2/Fe_3O_4 nanoparticles by stirring in the dark. As seen in supplementary figure (sfig. 1), the concentration of selenites was reduced by 17.5% for about 20 min mixing, after which no further significant reduction was observed. Since the concentration was decreased due to the adsorption of selenites on the particle surface, the net photocatalytic reduction was measured after subtracting the dark adsorption.

Since pK_1 and pK_2 for selenous acid are known to be 2.35-2.46 and 7.31-7.94, respectively, selenium cations mostly existed in the form of $HSeO_3^-$ at pH 4. The stability of the coated TiO_2 layer at this pH was confirmed by measuring the dissolved Ti concentration after mixing for 5 h using ICP-MS.

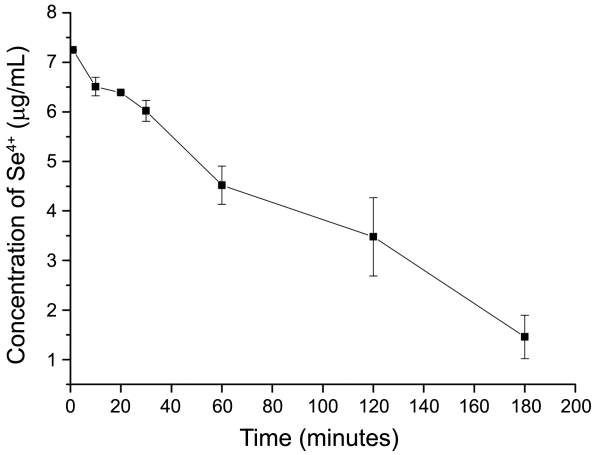

Figure 4. Photocatalytic reduction of selenite according to UV irradiation time. Conditions: 1.0 g/L of synthesized TiO_2@SiO_2/Fe_3O_4 nanoparticles, dark adsorption for 20 minutes, 300 mg/L of formic acid, pH 4.0, and initial selenite concentration of 8.0 μg/mL.

Photocatalytic Reduction of Selenite. For selenite reduction, 20 μg/mL of selenite synthetic standard solution was mixed with the nanoparticles and then irradiated by UV light for 20 min. Since the reduced selenium atoms after the reaction were adsorbed on the surface of the TiO_2 layer, the reaction sites on the surface became smaller and smaller, which reduced photocatalytic activity. Therefore, the number of nanoparticles should be sufficiently large compared to the selenite, otherwise the reaction rate will be gradually decreased. As shown in Figure 4, unlike the dark adsorption, the concentration of selenite was continuously decreased and the rate, equivalent to the slope, remained almost constant throughout the experiment as the irradiation time increased. This result indicated that a sufficient amount of nanoparticles was reacted in the solution. In detail, the amount of photoreduced selenite was measured by determining the selenium in the solution by ICP-MS. When 8.0 μg/mL selenite was reacted with 1.0 g/L of nanoparticles, 7.25 μg/mL of selenite was estimated at the beginning of the reaction after subtracting the dark adsorption. The measured selenite concentration was continuously decreased to 1.35 μg/mL after 180 min indicating a reduction of 81.4% after 3 h photoreaction. After reduction, the magnetic nanoparticles with the adsorbed selenium atoms were collected by a magnetic separation, and then washed three times with deionized water.

Photocatalytic Reduction of Selenate and Selenide. In case of selenate, the standard reduction potential was +1.060 V, which was higher than that of selenite. However, unlike selenite, almost no photocatalytic reduction of selenate was observed at this condition (supplementary sfig. 2) because of the relatively slow kinetics and low radiation power of the UV source (6 Watt) that limited the reduction of Se^{6+} to Se^{4+}.[24] About 4.7 to 4.8 μg/mL of selenate was determined when 5.0 μg/mL of selenate was mixed with the synthesized nanoparticles and irradiated for 3 h. In addition, no signal

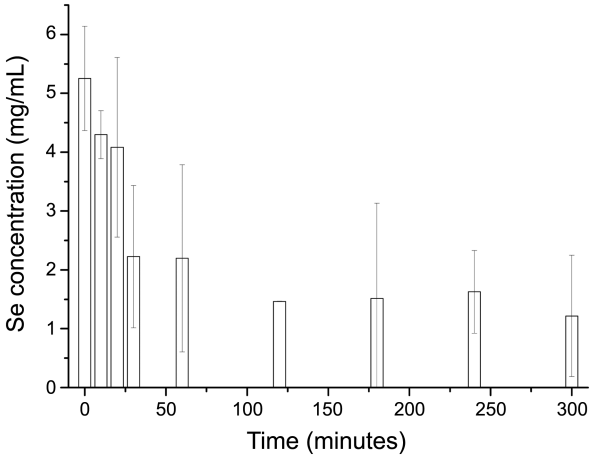

Figure 5. Photocatalytic reduction of selenite and selenide. Conditions: 0.5 g/L of nanoparticles, dark adsorption for 20 minutes, 300 mg/L formic acid as a hole scavenger, pH 4.0, 5.0 μg/mL of Se^{4+} and 1.6 μg/mL of Se^{2-}.

change of selenium at the collected nanoparticles was observed except for the dark adsorption. For organic selenide, no signal increase of the adsorbed selenium on the nanoparticles was observed, indicating the absence of any dark adsorption or photoreaction. This experimental study produced important technical information on speciation and separation. The speciation and preconcentration of selenium cations can be achieved by photocatalytic reaction of TiO_2 in the presence of UV. Furthermore, Se^{4+} can be separated from not only selenium anion or organic selenium, but also from Se^{6+} at this low UV power of 6 watt.

For further confirmation, the mixture of selenite and selenide was photoreduced and the analytical result of ICP-MS is shown in Figure 5. During the initial 1 h, much of the selenite was removed, after which the reduction rate was greatly reduced for the next 2 h to give a constant concentration after 3 h, which indicated completion of the photocatalytic reduction within 3 h.

Conclusions

The separation of selenite from selenate and selenide using synthesized TiO_2@SiO_2/Fe_3O_4 nanoparticles was successfully demonstrated for the first time. The nanoparticles showed good stability throughout the experiment. The superparamagnetic property of the Fe_3O_4 core was useful to separate and preconcentrate the reduced selenium atoms adsorbed on the particle surface. The photocatalytic property of TiO_2 shell reduced the selenite efficiently. The photocatalytic reduction depended on the power of the UV radiation source and on the reaction time. Noticeably Se^{4+} can be separated from not only selenium anion or organic selenium, but also Se^{6+}, at the low radiation power of 6 watts due to the slower kinetics of Se^{6+} compared to that of Se^{4+}. The developed method using the synthesized TiO_2@SiO_2/Fe_3O_4 nanoparticles can provide a convenient and unique tool for the separation of selenium cations from anions or organic selenium in environmental and biological samples.

Acknowledgments. This work was supported by the Internal Research Fund of Dankook University (2012).

References

1. Uden, P. C. *Anal. Bioanal. Chem.* **2002**, *373*, 422.
2. Zheng, J.; Ohata, M.; Furuta, N.; Kosmus, W. *J. of Chromatogr. A* **2000**, *874*, 55.
3. Li, S. X.; Deng, N. S. *Anal. Bioanal. Chem*. **2002**, *374*, 1341.
4. Gomez-Ariza, J. L.; Sanchez-Rodas, D.; Caro de la Torre, M. A.; Giraldez, I.; Moralez, E. J. *Chromatogr. A* **2000**, *889*, 33.
5. Tang, X.; Xu, Z.; Wang, J. *Spectrochim. Acta B* **2005**, *60*(12), 1580.
6. Tan, T. T. Y.; Beydoun, D.; Amal, R. *J. Phys. Chem. B* **2003**, *107*, 4296.
7. Tan, T. T. Y.; Beydoun, D.; Amal, R. *J. Photochem. Photobiol. A: Chem*. **2003**, *159*, 273.
8. Kikuchi, E.; Sakamoto, H. *J. Electrochem. Soc*. **2000,** *147*(12), 4589.
9. Tan, T. T. Y.; Zaw, M.; Beydoun, D.; Amal, R. *J. Nanoparticle Res*. **2002**, *4*(6), 541.
10. Malato, S.; Fernandez-Ibañez, P.; Maldonado, M. I.; Blanco, J.; Gernjak,W. *Catal. Today* **2009**, *141*, 1.
11. Herrmann, J. M. *Top. Catal*. **2005**, *34*, 49.
12. Watts, R. J.; Kong, S.; Lee, W. *J. Environ. Eng*. **1995**, *121*, 730.
13. Fernandez-Ibañez, P.; Blanco, J.; Malato, S.; de las Nieves, F. *J. Water Res*. **2003**, *37*, 3180.
14. Blanco, J.; Fernandez-Ibañez, P.; Malato, S. J. *Sol. Energy Eng*. **2007**, *129*, 4.
15. Alvareza, P. M.; Jaramilloa, J.; Lopez-Piñeroa, F.; Plucinski, P. K. *Applied Catalysis B: Environmental* **2010**, *100*, 338.
16. Xu, S.; Shangguan, W.; Yuan, J.; Chen, M.; Shi, J. *Appl. Catal. B: Environ*. **2007**, *71*, 177.
17. Abramson, S.; Srithammavanh, L.; Siaugue, J. M.; Horner, O.; Xu, X.; Cabuil, V. *J. Nanoparticle Res.* **2009**, *11*, 459.
18. Beydoun, D.; Amal, R.; Low, G. K. C.; McEvoy, S. *J. Phys. Chem. B* **2000**, *104*, 4387.
19. Beydoun, D.; Amal, R.; Scott, J.; Low, G.; McEvoy, S. *Chem. Eng. Technol*. **2001**, *24*, 745.
20. Beydoun, D.; Amal, R. *Mater. Sci. Eng*. **2002**, *94*, 71.
21. Watson, S.; Scott, J.; Beydoun, D.; Amal, R. *J. Nanoparticle Res.* **2005**, *7*, 691.
22. Jang, J. H.; Lim, H. B. *Microchem. J.* **2010**, *94*, 148.
23. Yu, H.; Irie, H.; Hashimoto, K. *J. Am. Chem. Soc*. **2010**, *132*, 6898.
24. Nguyen, V. N. H.; Beydoun, D.; Amal, R. *J. Photochem. Photobiol. A: Chem.* **2005**, *171*, 113.